Morphology and Electronic Properties of Electrochemically Exfoliated Graphene

Matilde Eredia,[†] Simone Bertolazzi,[†] Tim Leydecker,[†] Mohamed El Garah,[†] Iwona Janica,[†,‡,§] Georgian Melinte,[‖] Ovidiu Ersen,[‖] Artur Ciesielski[†,] and Paolo Samorì[†,]**

† Université de Strasbourg, CNRS, ISIS, 8 allée Gaspard Monge, 67000 Strasbourg, France.

‡ Centre for Advanced Technologies, Adam Mickiewicz University, Umultowska 89c, 61-614 Poznań, Poland.

§ Faculty of Chemistry, Adam Mickiewicz University, Umultowska 89b, 61614 Poznan, Poland.

‖ Institut de Physique et Chimie des Matériaux de Strasbourg (IPCMS), 23 rue du Loess, 67037 Strasbourg, France.

*A.C. ciesielski@unistra.fr, P.S. samori@unistra.fr

Abstract

Electrochemically exfoliated graphene (EEG) possesses optical and electronic properties that are markedly different from those of the more explored graphene oxide both in its pristine and reduced forms. EEG also holds the unique advantage compared to other graphenes produced by exfoliation in liquid media: it can be obtained in large quantities in a short time. However, an in-depth understanding on the structure-properties relationship of this material is still lacking. In this work, we report a physico-chemical characterization of EEG combined with an investigation on the electronic properties of this material carried out both at the single flake level and on the films. Additionally, we use for the first time microwave irradiation to reduce the EEG and demonstrate that the oxygen functionalities are not the bottleneck for charge transport in EEG, which is rather hindered by the presence of structural defects within the basal plane.

TOC GRAPHICS

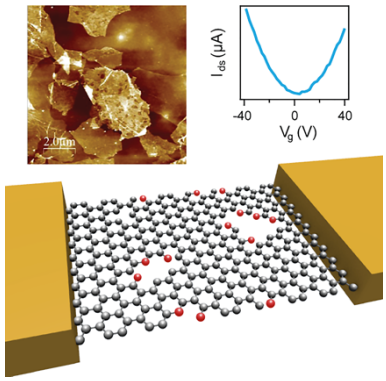

Graphene, a monolayer of carbon atoms arranged in a hexagonal lattice, is the most explored two-dimensional (2D) material.[1] Graphene is atomically thin, ultra-light, highly transparent, and it possesses extraordinary electronic[2-3] and thermal properties.[4] All these superlatives make graphene a promising material for many applications as transparent conducting film,[5] as electrode in supercapacitors,[6-7] as active layer in sensors,[8-9] etc. Nevertheless, the physico-chemical properties of graphene closely depend on the way it is produced and processed. Although the highest quality graphene sheets can be prepared *via* mechanical exfoliation, i.e. through the "scotch-tape" approach, this method is not suitable for mass production to potentially enable the employment of graphene in daily life applications and devices. Recently, the community perceives an outbreak of new potentially upscalable methods of graphene production. Among them, the ultrasound-induced liquid-phase exfoliation (UILPE)[10-11] of graphite in the absence[12] or presence of *ad hoc* molecules,[13-16] and the electrochemical exfoliation (EE) carried in a variety of electrolytes[17,18-19] are extensively explored as they can be used to produce graphene flakes of different sizes, thicknesses and quality. Significantly, while the UILPE makes it possible to produce dispersions with the maximum concentration of 1 mg/mL[20] and it requires long (up to 1000 hours) sonication processes and multi-step post treatments, the electrochemically exfoliation allows to generate 1-10 mg/mL dispersions in the time scale spanning from minutes to a few hours.[21] Interestingly, EE of graphite into graphene can occur either under anodic or cathodic conditions.[19] While cathodic exfoliation relies on the use of lithium or alkylammonium salts dissolved in organic solvents (e.g. propylene carbonate,[22] dimethyl sulfoxide,[23] N-methyl-2-pyrrolidone[18]), the anodic process can be carried out in aqueous media. Various aqueous electrolytes[17, 24-26] as well as mixtures of water and ionic liquids[27-28] have been investigated. Among them aqueous electrolytes containing inorganic sulfate

salts became extremely popular for their good performance, which results in the high-yield exfoliation of graphene sheets.[21]

Owing to the oxidative nature of the anodic exfoliation process, many research groups have proposed this method as an alternative to classical Hummers and Staudenmaier methods for the production of graphene oxide (GO).[29-32] On the other hand, contradicting reports have appeared in the last few years[17, 24-25, 33-35] in which electrochemical exfoliation of graphite was used to produce defect-free graphene sheets at high concentrations. In fact, the oxidation of graphene sheets is unavoidable during the anodic EE, and it depends on both the exfoliation time and the type of employed electrolyte, which in some cases can prevent the extensive oxidation.[33, 36] While the production of high quantity of defect-free graphene sheets *via* wet methods attracts the attention of both industrial and academic sectors,[37] besides the oxidation degree little is known on the physico-chemical properties of electrochemically exfoliated graphene (EEG) sheets, such as the nature of the defects and electronic properties at the single sheet and film level. Although EE in non-aqueous electrolytes prevents the extensive oxidation of graphitic material, which characterizes the anodic process, cathodic EE requires time consuming post treatments of the exfoliated materials, such as long ultra-sonication, employed to achieve compete exfoliation and therefore, has the same drawbacks as UILPE, i.e. low exfoliation yield and limited lateral sizes of the flakes (in the range of hundreds of nm)[14]. Because of this reason, current research endeavors are focused on the anodic approach, which, on the contrary, allows the one-step production of single- and few-layered graphene sheets in high quantities. In particular, it has been shown recently that devices based on the thin EEG film possess a maximum hole mobility of ca. 100 $cm^2\ V^{-1}\ s^{-1}$, whereas single-layer (SL) EEG exhibits a hole mobility of ca. 300 $cm^2\ V^{-1}\ s^{-1}$ and a sheet resistance of 2 $k\Omega\ sq^{-1}$,[17] being comparable to that of

undoped CVD-grown graphene (1 kΩ sq^{-1}).[38] Such low mobility (if compared to pristine graphene)[2, 39] has been provisionally attributed to the inter-flakes boundaries, which are bottlenecks for charge transport, and to the presence of the oxygen functionalities in the structure of the flakes, the latter acting as electronic traps. However, an in-depth analysis on the structure-properties relationship in EEG, by comparing the electrical characteristics of this 2D material measured at the single flake and at the film level, in device with variable oxygen content is missing.

Here we show that the electrochemical exfoliation of graphite foil under the most commonly employed anodic conditions,[17, 24, 29-30, 34, 36, 40-42] i.e. using ammonium sulfate as electrolyte, not only causes the oxidation of the graphitic material, but also results in the structural degradation of the sheets. In particular, structural and compositional characterization of the produced material corroborated with the investigation on the electronic properties of both SL flakes and films provide unambiguous evidence that the electrical characteristics of EEG are not hindered by the amount of oxygen functionalities, which can be nearly completely removed upon microwave (MW) irradiation, but are rather limited by the presence of structural defects.

In this work, EEG has been produced under anodic conditions using a simple electrolytic cell (see *Experimental Section*). During the electrolysis, the area of the working electrode, i.e. graphite foil, is being reduced determining a variation of the current intensity passing between the electrodes. Noteworthy, a prolonged electrolysis in aqueous solution affects the oxidation degree of the produced material as observed by following the C/O ratio as a function of the electrolysis duration (Figure S1a). In particular, an electrolysis process lasting 1 and 60 min results in a C/O ratio of 8 and 4, respectively. Therefore, we decided to focus our attention on the

EEG characterized by the highest C/O ratio (C/O = 8), i.e. the material collected after 1 minute of electrolysis.

Such EEG is characterized from the physical-chemical point of view by various microscopic and spectroscopic techniques. A fast preliminary investigation can be attained by optical microscopy (OM), which allows quick determination of the presence of single- and few-layer thick graphene flakes deposited on the SiO_2 substrate. Subsequently, an in-depth morphological characterization of the exfoliated material is performed. In particular, statistical distributions of flake size and thickness are determined by atomic force microscopy (AFM) and high-resolution transmission electron microscopy (HR-TEM). Figure 1a displays large single-layer graphene (SLG) and few-layer graphene (FLG) sheets. Moreover, in a number of cases folded or wrinkled sheets are also monitored, being commonly observed in samples prepared by wet deposition methods such as spin-coating. AFM and HR-TEM analyses (Figure S3) reveal a considerable fraction of folded SLG sheets with lateral sizes > 1 μm, being a typical characteristic of graphene produced *via* EE.[17, 24, 42] The thickness distribution (see Figure 1b) quantified by AFM and HR-TEM reveals a discrepancy which is a consequence of the intrinsic nature of the measurements. In particular, while in the case of HR-TEM the number of layers (*N*) is counted by analysing the folded edges,[43] AFM enables the estimation of *N* by measuring the height of the deposited flakes from topographical profiles and dividing it by the graphite interlayer distance. Moreover, it is worth noting that the estimation of the height of a SLG *via* AFM depends on the substrate and on the experimental conditions such as relative humidity and magnitude of the force applied by the tip to the sample. For example, on SiO_2, a SLG can show an apparent height of ca. 1 nm,[44] while on mica it amounts to ca. 0.4 nm.[45] Here, the *N* is estimated by assuming that the apparent thickness of the thinnest graphene sheet observed on our images, amounting to 0.8 nm.

Interestingly, all the flakes analysed with AFM are less than 3.2 nm thick; therefore, the thickest flakes are considered to be four-layer thick. Both analyses, i.e. AFM and HR-TEM, show that EEG is mostly composed by SLG and bi-layer graphene sheets.

AFM is also employed to gain in-depth insight into the surface morphology of EEG flakes. High magnification imaging reveals that the surface of the flakes is damaged and nanoscopic holes are observed (Figure 1d). The density of those defects is estimated by automatic pixel counting. Such analysis shows that the defective area of the flakes ranges from 4 to 30% (see Figure 1e), yet, it does not exceed 10% for the majority of the flakes (67%).

Several attempts to visualize such structural defects by HR-TEM are done, yet the imaging is hindered by a contamination with physisorbed carbonaceous material, which after exposure to TEM electron beam converts into amorphous carbon. According with AFM imaging, in fact, most of the EEG flakes appear damaged and characterized by rough surfaces. That can be interpreted as the result of a non-uniform disintegration of the outer sheets in bi- and tri-layer thick flakes due to the complicated interplay of water electrolysis, anionic intercalation, and gas evolution that can induce cracks and nanoscopic defects on the material. Therefore, we believe that the main source of carbon contamination is represented by the remaining shreds of the external graphene layer of an EEG sheet, which are transformed in amorphous carbon under the influence of the electron beam. On the other hand, besides the nanoscopic defects observed by AFM, the HR-TEM analysis highlights the presence of point defects (Figure S3d).

The mechanical pressure caused by gas bubbling (O_2 and SO_2) in between graphite layers during the electrolysis is considered the most important factor leading simultaneously to the fragmentation and exfoliation of the material. That causes also the spreading of the graphitic

material from the anode, even before the complete exfoliation, which in fact is well reflected in the heterogeneity over the thickness and sizes of the produced material (Figures 1b and 1c).

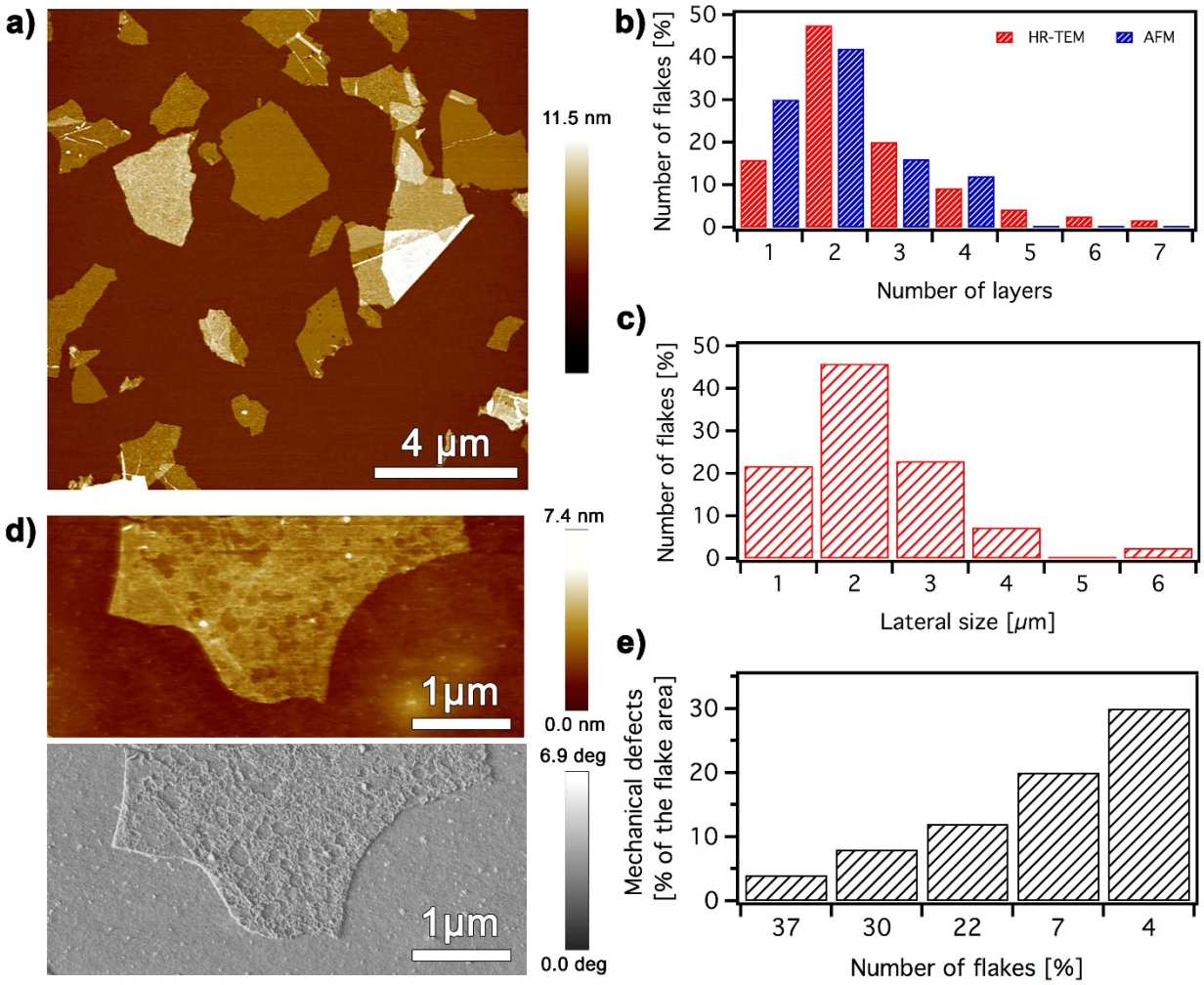

Figure 1. Statistical thickness and flake size analysis for electrochemically exfoliated graphene, together with a statistical study of structural defects caused by the electrochemical process. (a) Topographical AFM image of flakes produced by electrochemical exfoliation of graphite and deposited on SiO_2 substrates by spin-coating from DMF dispersions; (b) distribution of the number of layers per sheet determined by AFM cross-sectional analysis (in blue) and HR-TEM (in red); (c) distribution of flakes lateral size determined by AFM; (d) AFM topographic

and phase-contrast images showing structural defects on a representative SLG flake; (e) density of the structural defects plotted in function of the number of defective flakes.

Compositional characterization of the material is carried out by X-ray photoelectron spectroscopy (XPS). Firstly the starting materials, i.e. the graphite foil, was analysed, and considered as standard, aiming to follow how the chemical composition of the material evolves during electrochemical exfoliation (see Figures S1b and S1c). Figure 2a displays a comparison between C1s spectra of the starting material and EEG. As previously reported,[46] the high-resolution C1s spectrum of the starting material (Figure 2b), displays an asymmetric peak centred at 284.48 eV and a broad "shake-up'' peak related to the π to π^* transition, at ca. 290.9 eV. No components related to the oxidation of the material is observed, as confirmed by the low atomic percentage of oxygen (0.58 %) given from the survey spectra (Figure S1b). After the exfoliation, the C1s spectrum of EEG powder (Figure 2c), besides the main peak centred at 284.45 eV reveals a second component at higher binding energy, which indicates the oxidation of the material during the EE. Its deconvolution allows identification of four peaks typically attributed to oxygen-containing groups, i.e. hydroxyl (285.47 eV) and epoxide (286.68 eV) groups, as well as carbonyl (288.22 eV) and carboxyl (289.08 eV) moieties.[47-48] Even though the electrochemical process, under anodic conditions, unavoidably oxidizes the material, the level of oxidation is much lower if compared with the oxidation degree of GO powder obtained after drying a water dispersion of GO, purchased from Graphenea, in a vacuum oven at ca. 30 °C (Figure 2). Moreover, the content of oxygen, and consequently the C/O ratio determined by XPS, is comparable with the results of elemental microanalyses (see Table S1). Further analysis is performed by attenuated total reflectance Fourier transform infrared spectroscopy (ATR-FTIR)

and thermogravimetric analysis (TGA), which further corroborates the presence of oxygen containing groups (Figures S2a and S2b).

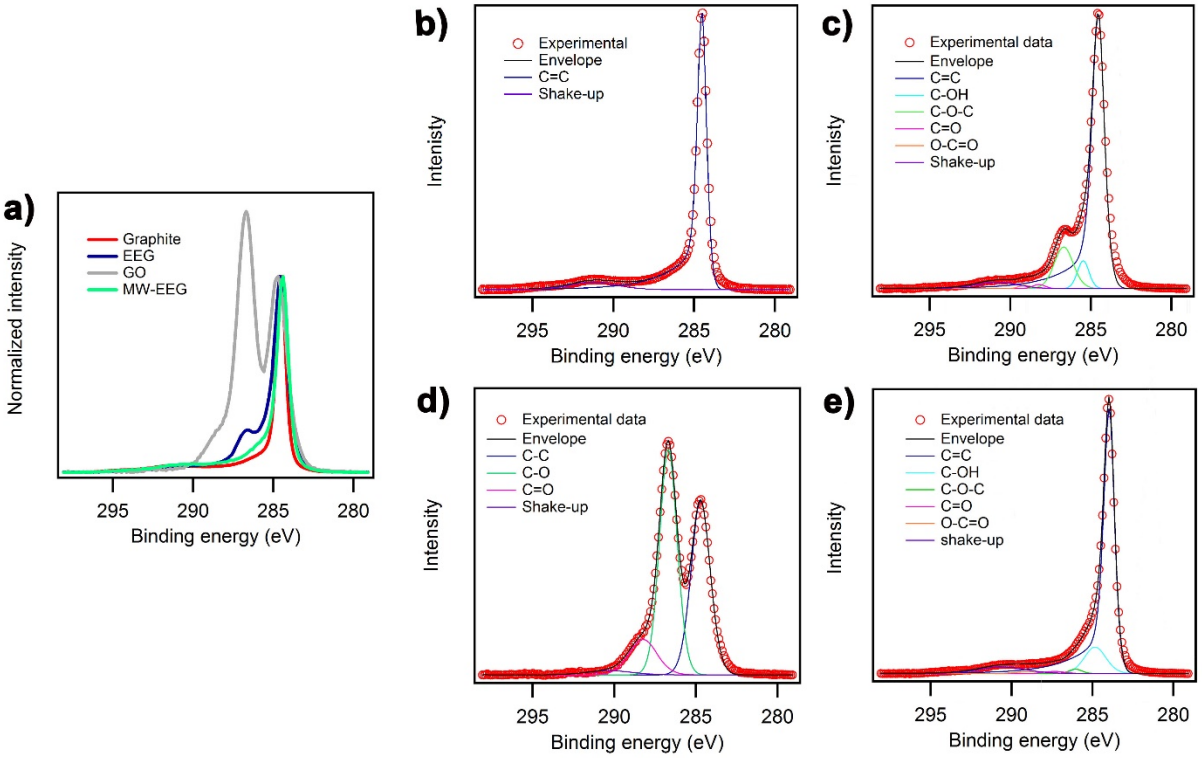

Figure 2. XPS characterization of electrochemically exfoliated graphene (EEG) in comparison with pristine graphite, graphene oxide (GO) and EEG after microwave irradiation (MW-EEG): (a) overlapped high resolution carbon spectra; (b) C1s spectrum of graphite; (c-e) C1s curve fitting of EEG, GO and MW-EEG, respectively.

Raman spectroscopy is used to characterize the quality of the EEG. The dispersions are spin-coated on SiO_2 substrates and the solvent is slowly evaporated at room temperature. Raman spectra (Figure S4c) show a disordered material as indicated by the presence of a defective peak higher than the G-peak and a very low intense and broad 2D band, providing evidence for a reduction of the size of the in-plane sp^2 domains subsequently to the anodic process. In

particular, I_D/I_G ratio of EEG (c.a. 1.5) lies in the transition region between stage 1 and 2, defined for disordered carbon materials, in which a mean distance between two defects is being estimated as $L_d \sim 2$-4 nm and consist of a low sp^3 species (<15%).[49] The position of G peak at 1593 cm^{-1} further proves the defective nature of EEG, which, in agreement with previous reports,[49-50] can be defined as nanocristalline graphite. Moreover, an apparent shoulder of the G peak, known as D' peak, can be clearly distinguished, indicating a moderate defect concentration.[51] Nevertheless, besides the defective flakes, high-quality FLG sheets, with I_D/I_G of 0.4, are observed.

Figure 3a, b illustrates the approach adopted for the electrical characterization of individual EEG nanosheets. EEG flakes are deposited on oxidized silicon substrates ($\varrho_{Si} \approx 0.001$ Ω·cm, $t_{ox} = 290$ nm) by spin-coating a 1 mg/mL dispersion in dimethylformamide (DMF), and are further characterized *via* a combination of OM and AFM. Multi-terminal back-gated field-effect transistors (FETs) are fabricated using e-beam lithography with polymethyl methacrylate (PMMA) resists, metal deposition (3/40 nm of Ti/Au) and lift off in acetone. The four-probe measurement configuration is employed to remove the contribution of the contact resistance and access the intrinsic sheet resistivity of EEG, which is found to span within the range 15-30 kΩ/sq. To minimize the influence of environmental adsorbates, such as O_2 and H_2O, all the measurements are carried under inert atmosphere (N_2-filled glovebox). Moreover, a vacuum-annealing step ($p \sim 5x10^{-8}$ mbar, $T \sim 60$ °C) is performed to desorb solvent traces, as well as O_2 and H_2O, which are known to be detrimental electron-acceptor traps ─ and thus reduce the level of hole doping within the material. Upon annealing, the behaviour of the EEG FETs changes from unipolar (*p*-type) to ambipolar, as in the case of mechanically exfoliated or CVD-grown graphene devices. A well-defined charge-neutrality point can be identified in the transfer

characteristics acquired after vacuum annealing (Figure 3c, inset) at V_g values of ~ 4 V. To the best of our knowledge, this is the first observation of ambipolar transport in EEG nanosheets, which proves that the level of oxidation in our EEG is considerably lower than in the case of graphene oxide (GO). However, at this stage, the electron and hole mobilities (1-10 $cm^2V^{-1}s^{-1}$) appear to be dominated by a high degree of structural defects, as elucidated in the following of the paper. The field-effect mobilities ─ measured in both two- and four-terminal configuration ─ are reported in the histogram in Figure 3d. On average, the two-terminal measurements provide mobility values 30-40% lower than the four-terminal counterpart, indicating a non-negligible contribution of the contact resistance due to injection barriers at the metal/EEG interface. Upon annealing, the hole field-effect mobility drops by ~50%. We suggest two plausible mechanisms behind such charge-transport degradation, namely the thermally-activated expansion of structural defects[52] and the remarkable decrease in hole density (see Supporting Section 4).

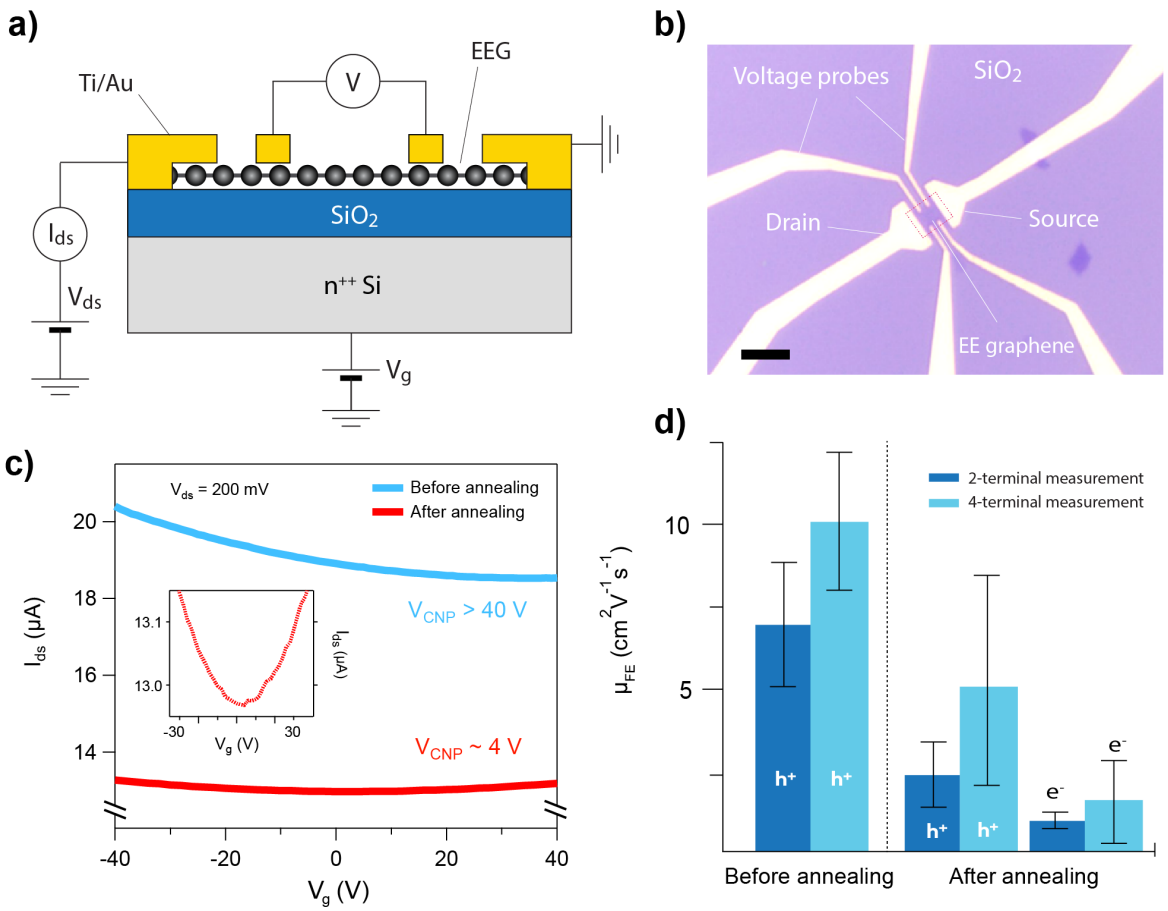

Figure 3. Electrical transport measurements on individual EEG flakes. (a) Schematics and (b) optical micrograph of the multiterminal back-gated FETs used for electrical characterization. The scale bar in (b) amounts to 5 μm. (c) Drain-source current (I_{ds}) *vs*. gate voltage (V_g) transfer characteristics of an EEG FET acquired before (blue) and after (red) high-vacuum annealing at ~60 °C. The curve is plotted also in the inset (magnified y-scale) to show the occurrence of the charge neutrality point (V_{CNP}) at ~4V. (d) Histogram of the field-effect mobility for holes (h+) and electrons (e-), as measured in the two- and four-terminal measurement configuration.

Graphene films are then prepared by depositing a few drops of EEG dispersion in DMF into a water-containing beaker. Once re-organized at the interface, EEG flakes form a uniform greyish film floating onto the sub-phase, which is transferred onto the solid substrate. This method

makes it possible to avoid time consuming and laborious purification steps, as a consequence of the EEG tendency to form a film at the water/air interface, leaving heavier particles, i.e. unexfoliated graphitic material diffusing in the sub-phase together with DMF. Therefore, the extensive formation of aggregates typical for other deposition methods such as drop-casting, dip-coating, spin-coating is avoided. Morphology and homogeneity of the films were investigated by OM (Figure S4a) and AFM (Figure 4b). Closely packed EEG sheets form large-area films having average thickness of about 3 nm and surface coverage above 80%. Gold source and drain electrodes are then evaporated on top of the film. The I_{ds} current is plotted as a function of the applied gate potential V_g and the resulting transfer curves are fitted in order to extract the mobility values in the linear regime.

Unlike what is observed in the case of single flake measurements, the electrical performances of films recorded before and after thermal annealing result being almost identical, displaying mobilities of 3.4 $cm^2 V^{-1} s^{-1}$ and 4 $cm^2 V^{-1} s^{-1}$, respectively. Electrical characterization also reveals a large shift in threshold voltage: the Dirac point is now at very high positive gate bias, even after annealing. This strong *p*-doping of the EEG film can be ascribed to the effect of trapped adsorbates (oxygen and solvent) between overlapped flakes, which cannot be easily desorbed and hamper the emergence of ambipolar transport.

Nevertheless, a percolation path for charges among adjacent flakes guarantees the conductivity of our film and proves the high-quality overlapping among sheets observed by microscopies. More importantly, EEG films show similar mobility values to those of the single flake. Therefore, albeit the observed mobilities remain below state of the art, our approach offers the exciting possibility of producing large-area graphene performing as an ideal large monolayer.

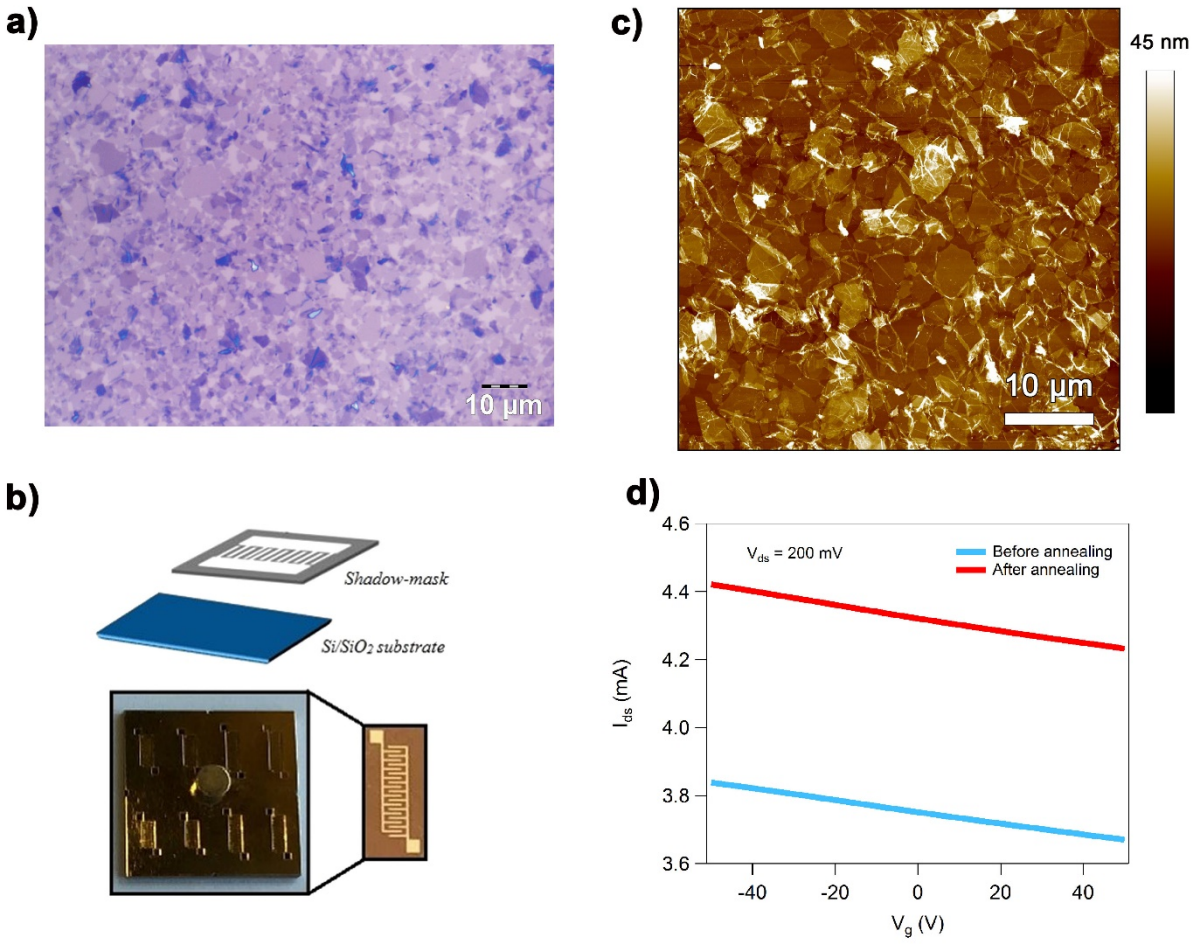

Figure 4. Electrical characterization of FETs based on EEG films. (a) Optical microscopy image and (b) AFM image of an EEG film; (c) sketch and photograph of the device fabrication on graphene films by gold evaporation using the shadow-mask approach; (d) representative transfer curves before and after annealing at 60 ºC for 12 h in nitrogen atmosphere. (V_{ds} = 200 mV)

Recently, microwave (MW) irradiation has been introduced as powerful technique to reduce graphene oxide achieving high-quality graphene.[53] Typically, (electro)chemical and thermal reduction of GO results in a highly defective and still oxidized material,[54-57] known as reduced graphene oxide (rGO), due to the difficulty of removing stable epoxy and carbonyl groups.[58] On the contrary, microwave treatments, based on a rapid and localized heating of the sample, causes

the desorption of oxygen functional groups as well as the reordering of the carbon atoms within the graphene basal plane, leading to defect- and oxygen-free graphene.[53] Consequently, electronic mobility values rise from 1 cm^2/Vs, reported for rGO[59-60], to 1000 cm^2/Vs after MW irradiation.[53]

Here, for the first time, this approach is exploited to lower the degree of oxidation on EEG and studying the effect on its electronic properties. While a preliminary thermal annealing is necessary to increase the conductivity of GO, so that it can absorb microwaves, this step was unnecessary in the case of EEG powder, which is successfully reduced upon a few seconds of microwaves irradiation with a conventional microwave oven (Figure 2a, green curve). As evident from the XPS survey spectra, the overall percentage of oxygen decreases from 12 % to 7 %. In particular, the C1s spectrum of EEG powder (Figure 2e) shows a nearly total reduction of epoxy and carbonyl groups to hydroxyl ones, as evidenced by the increase in –OH peak intensity. The shake-up satellite peak observed at 290.59 eV in MW-EEG spectrum indicates that the conjugation of the system is preserved and eventually restored as well. Moreover, the global shift of peak-maxima back to lower binding energy after MW irradiation points out the increment of the conducting nature of the material. We verified that the approach reported in literature[53] effectively reduces both EEG powder and EGG films on silicon dioxide substrates (Figure S5).

Surprisingly, when MW treatment is performed on EEG films, no noticeable changes in electrical performances are observed (see Figure S4d). While these results can be well explained by the Raman spectra on the films EEG before and after MW treatments, which appear very similar (Figure S4c), the C1s region of the XPS spectra shows that the MW treatment is accompanied with lowering of the peak at ca. 286 eV which is associated to oxygen-containing groups (Figure S4b). Although the combination of thermal annealing and microwave irradiation

of GO is known to be beneficial to the healing of point defects,[53] our nanometer sized structural defects cannot be recovered in the same way upon MW. As a result, MW-irradiation is not effective in recovering the electronic properties of EEG, which are at this stage limited by the presence of structural defects.

In summary, in this work we investigated the correlation between structure and electrical characteristics in electrochemically-exfoliated graphene.

Stable dispersions of graphene were prepared by means of the electrochemical approach using ammonium sulphate as electrolyte. We have carried out a multiscale characterization of the physico-chemical properties of EEG, in order to cast light onto the factors that influence the charge-carrier transport in this material. Taking advantages of the micrometer size of graphene flakes, multi-terminal FETs based on single flakes were fabricated allowing measuring mobilities of 1-10 $cm^2V^{-1}s^{-1}$ at the single flake level. Such mobilities turned out to be very similar to those measured on continuous EEG films. Interestingly, we have reported for the first time the emergence of the *n*-conductivity in EEG upon thermal annealing, leading to an ambipolar transport, which may be of interest for the development of logic circuits. We have also showed that MW treatments can be successfully exploited on EEG in order to lower the oxygen content, enabling to demonstrate that charge transport within EEG is mostly hindered by structural defects rather than by oxygen containing defects. Such novel information can be useful for the optimization of the graphene's electrochemical-exfoliation process, which is at present the most promising method for the production of high-quality graphene sheets in large quantities and short time.

Experimental Methods

Materials. Graphite foil (Alfa Aesar, 0.5 mm thick) was cut into pieces of 2.5 cm x 8 cm and used as anode and source of graphene for electrochemical process, while a platinum wire (GoodFellow, diameter of 0.5 mm) was employed as counter electrode. Ammonium sulfate was purchased from Sigma Aldrich and used as electrolyte in aqueous solution. N,N-Dimethylformamide (Sigma Aldrich) was used for preparing graphene dispersions. Substrates for characterization and devices preparation were purchased from Fraunhofer Institute and consist of n++-Si substrates with 90 (or 290) nm of thermally grown SiO_2 as the gate dielectric.

Electrochemical exfoliation of graphite foil. A simple electrolytic cell was built using few basic components such as a platinum wire as cathode and a graphite foil as anode half-immersed in an electrolytic solution. The electrolyte was prepared solubilizing in water the stoichiometric amount of $(NH_4)_2SO_4$ needed to reach a concentration of 0.1 M. The working electrode's exfoliation occurs as immediate consequence of the applied voltage between the two electrodes e.g. +15 V (ISO-TECH IPS-603 DC power supply), which generate a starting current of ca. 0.4A. Produced powder was collected by vacuum filtration on PTFE membranes (pores' diameter of 5 μm) and, after several rinsing steps needed to remove salt residuals, it was dispersed in DMF by mild sonication for 20 minutes. Such dispersion was kept to decant for 48 h in order to promote the sedimentation of un-exfoliated material.

Sample preparation. All the substrates were cleaned by subsequent ultrasonication in acetone and isopropyl alcohol (30 minutes each), in order to wash off the protective photoresist layer, and then dried under nitrogen flow. Afterward, the substrates were treated by UV-O_3 for 5 minutes followed by 25 minute of exhaust. The samples for optical microscopy imaging, AFM,

Raman and single flakes characterization were prepared by spin-coating onto SiO_2 substrates of a graphene dispersion at a concentration of 1 mg/mL in DMF.

EEG films were prepared starting from pristine dispersion in DMF where EEG thin layers are well stabilized. Few drops of dispersion were gently spread on water surface. Once re-organized at the interface, thin flakes form a uniform greyish film floating onto the sub-phase. The transfer was done dipping the SiO_2 substrate at 45 degrees in order to fish the film formed at the liquid-air interface.

The samples for HR-TEM analysis were prepared by drop-casting on a lacey carbon-coated copper grid and drying at room temperature.

Characterization of produced materials. A preliminary investigation of the samples was performed by optical microscopy, followed by morphological characterization by atomic force microscopy (AFM). AFM imaging was carried out using a Veeco Dimension 3100 atomic force microscope operating on a Nanoscope IV control unit under ambient condition. Topographic and phase imaging was performed operating in tapping mode using antimony (n) doped silicon cantilever. Thickness and surface coverage of the EEG films were determined by analysis of AFM images.

Optical microscopy images were recorded by Olympus BX51.

HR-TEM micrographs were taken on a FEI Tecnai F20 TEM equipped with a Schottky emitter and operated at 120 keV. The number of graphene layers was estimated from the number of (0,0,2) diffraction fringes at the edge of folded graphene sheets. The samples were prepared by drop-casting on a lacey carbon copper grid, followed by solvent evaporation.

XPS analysis were carried out using a Thermo Scientific K-Alpha X-ray photoelectron spectrometer equipped with an aluminium X-ray source (energy 1.4866 keV) and working at

pressure of 10^{-8}-10^{-9} mbar in the main chamber. X-ray spot size was settled at 400 μm. Survey spectra were recorded as result of 10 scans with a pass energy of 200.00 eV and a step size of 1 eV; high-resolution spectra are average of 10 scans with a pass energy of 50.00 eV and a step size of 0.1 eV. The material was analysed both in form of powder, after drying it for 48 h in dessicator, and as film deposited on native silicon wafers.

The IR analysis was carried out using infra Rouse Nicolet 6700 with MCT/A detector. The material was analysed in form of powder, dried in desiccator.

Raman spectra were recorded by a Renishaw microscope with a 100x objective, laser excitation wavelength of 532 nm and laser power of 1%. The silicon peak at 520.3 cm^{-1} was took as reference for wavenumber calibration.

Device preparation. Top-contact bottom gate FETs based on EEG film were fabricated depositing EEG film on silicon substrates with a 90 (or 230) nm silicon oxide layer and evaporating gold electrodes (70 nm thick) on top of graphene film by shadow mask method. Multiterminal back-gated field-effect transistors (FETs) based on single flake are fabricated using standard e-beam lithography, metal deposition (3/40 nm of Ti/Au) and lift off.

Electrical characterization. Devices with different channel length (120, 100, 80, 60 μm) between source and drain electrodes and W=10,000 μm (oxide thickness = 90 nm) were tested. The electrical measurements were performed in glove box under N_2 atmosphere.

ASSOCIATED CONTENT

Supporting Information. The Supporting Information is available free of charge on the ACS Publications website at DOI: XXX

Chemical analyses of electrochemically exfoliated material, High-resolution TEM, Microwave treatment of EEG films (XPS, Raman spectroscopy, electrical characterization).

AUTHOR INFORMATION

Corresponding Authors

*(A.C.) E-mail: ciesielski@unistra.fr

*(P.S.) E-mail: samori@unistra.fr

Notes

The authors declare no competing financial interest.

ACKNOWLEDGMENT

We acknowledge financial support from the IRTG Soft Matter Science, the European Commission through the Graphene Flagship (GA-696656), the Agence Nationale de la Recherche through the LabEx project Nanostructures in Interaction with their Environment (ANR-11-LABX-0058_NIE), the International Center for Frontier Research in Chemistry (icFRC) and Polish National Science Center (Grant. No. 2015/18/E/ST5/00188).

References

(1) Ferrari, A. C.; Bonaccorso, F.; Fal'ko, V.; Novoselov, K. S.; Roche, S.; Boggild, P.; Borini, S.; Koppens, F. H. L.; Palermo, V.; Pugno, N., *et al*. Science and Technology Roadmap for Graphene, related Two-Dimensional Crystals, and Hybrid Systems. *Nanoscale* **2015**, *7*, 4598-4810.

(2) Mayorov, A. S.; Gorbachev, R. V.; Morozov, S. V.; Britnell, L.; Jalil, R.; Ponomarenko, L. A.; Blake, P.; Novoselov, K. S.; Watanabe, K.; Taniguchi, T.*, et al*. Micrometer-Scale Ballistic Transport in Encapsulated Graphene at Room Temperature. *Nano Lett*. **2011**, *11*, 2396-2399.
(3) Fiori, G.; Bonaccorso, F.; Iannaccone, G.; Palacios, T.; Neumaier, D.; Seabaugh, A.; Banerjee, S. K.; Colombo, L. Electronics Based on Two-Dimensional Materials. *Nature Nanotech*. **2014**, *9*, 768-779.
(4) Balandin, A. A. Thermal Properties of Graphene and Nanostructured Carbon Materials. *Nat. Mater*. **2011**, *10*, 569-581.
(5) Biswas, S.; Drzal, L. T. A Novel Approach to Create a Highly Ordered Monolayer Film of Graphene Nanosheets at the Liquid-Liquid Interface. *Nano Lett*. **2009**, *9*, 167-172.
(6) Wu, Z. S.; Liu, Z. Y.; Parvez, K.; Feng, X. L.; Müllen, K. Ultrathin Printable Graphene Supercapacitors with AC Line-Filtering Performance. *Adv. Mater*. **2015**, *27*, 3669-3675.
(7) Bonaccorso, F.; Colombo, L.; Yu, G. H.; Stoller, M.; Tozzini, V.; Ferrari, A. C.; Ruoff, R. S.; Pellegrini, V. Graphene, Related Two-Dimensional Crystals, and Hybrid Systems for Energy Conversion and Storage. *Science* **2015**, *347*, 1246501.
(8) Schedin, F.; Geim, A. K.; Morozov, S. V.; Hill, E. W.; Blake, P.; Katsnelson, M. I.; Novoselov, K. S. Detection of Individual Gas Molecules Adsorbed on Graphene. *Nat. Mater*. **2007**, *6*, 652-655.
(9) Shao, Y. Y.; Wang, J.; Wu, H.; Liu, J.; Aksay, I. A.; Lin, Y. H. Graphene Based Electrochemical Sensors and Biosensors: A Review. *Electroanal* **2010**, *22*, 1027-1036.
(10) Hernandez, Y.; Nicolosi, V.; Lotya, M.; Blighe, F. M.; Sun, Z. Y.; De, S.; McGovern, I. T.; Holland, B.; Byrne, M.; Gun'ko, Y. K.*, et al*. High-Yield Production of Graphene by Liquid-Phase Exfoliation of Graphite. *Nat. Nanotechnol*. **2008**, *3*, 563-568.
(11) Lotya, M.; Hernandez, Y.; King, P. J.; Smith, R. J.; Nicolosi, V.; Karlsson, L. S.; Blighe, F. M.; De, S.; Wang, Z. M.; McGovern, I. T.*, et al*. Liquid Phase Production of Graphene by Exfoliation of Graphite in Surfactant/Water Solutions. *J. Am. Chem. Soc*. **2009**, *131*, 3611-3620.
(12) Du, W. C.; Jiang, X. Q.; Zhu, L. H. From Graphite to Graphene: Direct Liquid-Phase Exfoliation of Graphite to Produce Single- and Few-Layered Pristine Graphene. *J. Mater. Chem. A* **2013**, *1*, 10592-10606.
(13) Ciesielski, A.; Samorì, P. Graphene *via* Sonication assisted Liquid-Phase Exfoliation. *Chem. Soc. Rev*. **2014**, *43*, 381-398.
(14) Ciesielski, A.; Samorì, P. Supramolecular Approaches to Graphene: From Self-Assembly to Molecule-Assisted Liquid-Phase Exfoliation. *Adv. Mater*. **2016**, *28*, 6030-6051.
(15) Ciesielski, A.; Haar, S.; El Gemayel, M.; Yang, H. F.; Clough, J.; Melinte, G.; Gobbi, M.; Orgiu, E.; Nardi, M. V.; Ligorio, G.*, et al*. Harnessing the Liquid-Phase Exfoliation of Graphene Using Aliphatic Compounds: A Supramolecular Approach. *Angew. Chem. Int. Ed*. **2014**, *53*, 10355-10361.
(16) Du, W. C.; Lu, J.; Sun, P. P.; Zhu, Y. Y.; Jiang, X. Q. Organic Salt-Assisted Liquid-Phase Exfoliation of Graphite to Produce High-Quality Graphene. *Chem. Phys. Lett* **2013**, *568*, 198-201.
(17) Parvez, K.; Wu, Z. S.; Li, R. J.; Liu, X. J.; Graf, R.; Feng, X. L.; Müllen, K. Exfoliation of Graphite into Graphene in Aqueous Solutions of Inorganic Salts. *J. Am. Chem. Soc*. **2014**, *136*, 6083-6091.

(18) Cooper, A. J.; Wilson, N. R.; Kinloch, I. A.; Dryfe, R. A. W. Single Stage Electrochemical Exfoliation Method for the Production of Few-Layer Graphene *via* Intercalation of Tetraalkylammonium Cations. *Carbon* **2014**, *66*, 340-350.
(19) Abdelkader, A. M.; Cooper, A. J.; Dryfe, R. A. W.; Kinloch, I. A. How to Get Between the Sheets: a Review of Recent Works on the Electrochemical Exfoliation of Graphene Materials from Bulk Graphite. *Nanoscale* **2015**, *7*, 6944-6956.
(20) Coleman, J. N. Liquid Exfoliation of Defect-Free Graphene. *Acc. Chem. Res.* **2013**, *46*, 14-22.
(21) Yang, S.; Lohe, M. R.; Müllen, K.; Feng, X. L. New-Generation Graphene from Electrochemical Approaches: Production and Applications. *Adv. Mater.* **2016**, *28*, 6213-6221.
(22) Xia, Z. Y.; Giambastiani, G.; Christodoulou, C.; Nardi, M. V.; Koch, N.; Treossi, E.; Bellani, V.; Pezzini, S.; Corticelli, F.; Morandi, V.*, et al*. Synergic Exfoliation of Graphene with Organic Molecules and Inorganic Ions for the Electrochemical Production of Flexible Electrodes. *Chempluschem* **2014**, *79*, 439-446.
(23) Abdelkader, A. M.; Kinloch, I. A.; Dryfe, R. A. W. Continuous Electrochemical Exfoliation of Micrometer-Sized Graphene Using Synergistic Ion Intercalations and Organic Solvents. *ACS Appl. Mater. Interfaces* **2014**, *6*, 1632-1639.
(24) Parvez, K.; Li, R. J.; Puniredd, S. R.; Hernandez, Y.; Hinkel, F.; Wang, S. H.; Feng, X. L.; Müllen, K. Electrochemically Exfoliated Graphene as Solution-Processable, Highly Conductive Electrodes for Organic Electronics. *ACS Nano* **2013**, *7*, 3598-3606.
(25) Chen, C. H.; Yang, S. W.; Chuang, M. C.; Woon, W. Y.; Su, C. Y. Towards the Continuous Production of High Crystallinity Graphene *via* Electrochemical Exfoliation with Molecular in Situ Encapsulation. *Nanoscale* **2015**, *7*, 15362-15373.
(26) Xia, Z. Y.; Pezzini, S.; Treossi, E.; Giambastiani, G.; Corticelli, F.; Morandi, V.; Zanelli, A.; Bellani, V.; Palermo, V. The Exfoliation of Graphene in Liquids by Electrochemical, Chemical, and Sonication-Assisted Techniques: A Nanoscale Study. *Adv. Funct. Mater.* **2013**, *23*, 4684-4693.
(27) Liu, N.; Luo, F.; Wu, H. X.; Liu, Y. H.; Zhang, C.; Chen, J. One-Step Ionic-Liquid-Assisted Electrochemical Synthesis of Ionic-Liquid-Functionalized Graphene Sheets Directly from Graphite. *Adv. Funct. Mater.* **2008**, *18*, 1518-1525.
(28) Najafabadi, A. T.; Gyenge, E. High-Yield Graphene Production by Electrochemical Exfoliation of Graphite: Novel Ionic Liquid (IL)-Acetonitrile Electrolyte with Low IL Content. *Carbon* **2014**, *71*, 58-69.
(29) Ambrosi, A.; Pumera, M. Electrochemically Exfoliated Graphene and Graphene Oxide for Energy Storage and Electrochemistry Applications. *Chem. Eur. J.* **2016**, *22*, 153-159.
(30) Sevilla, M.; Ferrero, G. A.; Fuertes, A. B. Aqueous Dispersions of Graphene from Electrochemically Exfoliated Graphite. *Chem.Eur. J.* **2016**, *22*, 17351-17358.
(31) Liu, J. L.; Yang, H. P.; Zhen, S. G.; Poh, C. K.; Chaurasia, A.; Luo, J. S.; Wu, X. Y.; Yeow, E. K. L.; Sahoo, N. G.; Lin, J. Y.*, et al*. A Green Approach to the Synthesis of High-Quality Graphene Oxide Flakes *via* Electrochemical Exfoliation of Pencil Core. *RSC Adv.* **2013**, *3*, 11745-11750.
(32) Abdelkader, A. M.; Kinloch, I. A.; Dryfe, R. A. W. High-Yield Electro-Oxidative Preparation of Graphene Oxide. *Chem. Commun.* **2014**, *50*, 8402-8404.
(33) Yang, S.; Bruller, S.; Wu, Z. S.; Liu, Z. Y.; Parvez, K.; Dong, R. H.; Richard, F.; Samorì, P.; Feng, X. L.; Müllen, K. Organic Radical-Assisted Electrochemical Exfoliation for the Scalable Production of High-Quality Graphene. *J. Am. Chem. Soc.* **2015**, *137*, 13927-13932.

(34) Munuera, J. M.; Paredes, J. I.; Villar-Rodil, S.; Ayan-Varela, M.; Pagan, A.; Aznar-Cervantes, S. D.; Cenis, J. L.; Martinez-Alonso, A.; Tascon, J. M. D. High Quality, Low Oxygen Content and Biocompatible Graphene Nanosheets Obtained by Anodic Exfoliation of Different Graphite types. *Carbon* **2015**, *94*, 729-739.
(35) Liu, J. L.; Poh, C. K.; Zhan, D.; Lai, L. F.; Lim, S. H.; Wang, L.; Liu, X. X.; Sahoo, N. G.; Li, C. M.; Shen, Z. X., *et al*. Improved Synthesis of Graphene Flakes from the Multiple Electrochemical Exfoliation of Graphite Rod. *Nano Energy* **2013**, *2*, 377-386.
(36) Munuera, J. M.; Paredes, J. I.; Villar-Rodil, S.; Ayan-Varela, M.; Martinez-Alonso, A.; Tascon, J. M. D. Electrolytic Exfoliation of Graphite in Water with Multifunctional Electrolytes: en Route towards High Quality, Oxide-Free Graphene Flakes. *Nanoscale* **2016**, *8*, 2982-2998.
(37) Bonaccorso, F.; Lombardo, A.; Hasan, T.; Sun, Z. P.; Colombo, L.; Ferrari, A. C. Production and Processing of Graphene and 2d Crystals. *Mater. Today* **2012**, *15*, 564-589.
(38) Kholmanov, I. N.; Magnuson, C. W.; Aliev, A. E.; Li, H. F.; Zhang, B.; Suk, J. W.; Zhang, L. L.; Peng, E.; Mousavi, S. H.; Khanikaev, A. B., *et al*. Improved Electrical Conductivity of Graphene Films Integrated with Metal Nanowires. *Nano Lett.* **2012**, *12*, 5679-5683.
(39) Novoselov, K. S.; Geim, A. K.; Morozov, S. V.; Jiang, D.; Zhang, Y.; Dubonos, S. V.; Grigorieva, I. V.; Firsov, A. A. Electric Field Effect in Atomically Thin Carbon Films. *Science* **2004**, *306*, 666-669.
(40) Yu, P.; Tian, Z. M.; Lowe, S. E.; Song, J. C.; Ma, Z. R.; Wang, X.; Han, Z. J.; Bao, Q. L.; Simon, G. P.; Li, D., *et al*. Mechanically-Assisted Electrochemical Production of Graphene Oxide. *Chem. Mater.* **2016**, *28*, 8429-8438.
(41) Hsieh, C. T.; Hsueh, J. H. Electrochemical Exfoliation of Graphene Sheets from a Natural Graphite flask in the presence of sulfate ions at different temperatures. *RSC Adv.* **2016**, *6*, 96015-96015.
(42) Su, C. Y.; Lu, A. Y.; Xu, Y. P.; Chen, F. R.; Khlobystov, A. N.; Li, L. J. High-Quality Thin Graphene Films from Fast Electrochemical Exfoliation. *ACS Nano* **2011**, *5*, 2332-2339.
(43) Ferrari, A. C.; Meyer, J. C.; Scardaci, V.; Casiraghi, C.; Lazzeri, M.; Mauri, F.; Piscanec, S.; Jiang, D.; Novoselov, K. S.; Roth, S., *et al*. Raman Spectrum of Graphene and Graphene Layers. *Phys. Rev. Lett.* **2006**, *97*, 187401.
(44) Novoselov, K. S.; Jiang, D.; Schedin, F.; Booth, T. J.; Khotkevich, V. V.; Morozov, S. V.; Geim, A. K. Two-Dimensional Atomic Crystals. *Proc. Natl. Acad. Sci. USA* **2005**, *102*, 10451-10453.
(45) Valles, C.; Drummond, C.; Saadaoui, H.; Furtado, C. A.; He, M.; Roubeau, O.; Ortolani, L.; Monthioux, M.; Penicaud, A. Solutions of Negatively Charged Graphene Sheets and Ribbons. *J. Am. Chem. Soc.* **2008**, *130*, 15802-15804.
(46) Briggs, D.; Riviere, J. C. *Practical Surface Analysis: By Auger and X-ray Photoelectron Spectroscopy*. Wiley New York: Chichester, 1983.
(47) Hsiao, M. C.; Liao, S. H.; Yen, M. Y.; Teng, C. C.; Lee, S. H.; Pu, N. W.; Wang, C. A.; Sung, Y.; Ger, M. D.; Ma, C. C. M., *et al*. Preparation and Properties of a Graphene Reinforced Nanocomposite Conducting Plate. *J. Mater. Chem.* **2010**, *20*, 8496-8505.
(48) Park, S.; An, J. H.; Piner, R. D.; Jung, I.; Yang, D. X.; Velamakanni, A.; Nguyen, S. T.; Ruoff, R. S. Aqueous Suspension and Characterization of Chemically Modified Graphene Sheets. *Chem. Mater.* **2008**, *20*, 6592-6594.
(49) Ferrari, A. C.; Robertson, J. Interpretation of Raman Spectra of Disordered and Amorphous Carbon. *Phys. Rev. B* **2000**, *61*, 14095-14107.

(50) Cancado, L. G.; Jorio, A.; Ferreira, E. H. M.; Stavale, F.; Achete, C. A.; Capaz, R. B.; Moutinho, M. V. O.; Lombardo, A.; Kulmala, T. S.; Ferrari, A. C. Quantifying Defects in Graphene *via* Raman Spectroscopy at Different Excitation Energies. *Nano Lett*. **2011**, *11*, 3190-3196.
(51) Eckmann, A.; Felten, A.; Mishchenko, A.; Britnell, L.; Krupke, R.; Novoselov, K. S.; Casiraghi, C. Probing the Nature of Defects in Graphene by Raman Spectroscopy. *Nano Lett*. **2012**, *12*, 3925-3930.
(52) Annett, J.; Cross, G. L. W. Self-Assembly of Graphene Ribbons by Spontaneous Self-Tearing and Peeling from a Substrate. *Nature* **2016**, *535*, 271-275.
(53) Voiry, D.; Yang, J.; Kupferberg, J.; Fullon, R.; Lee, C.; Jeong, H. Y.; Shin, H. S.; Chhowalla, M. High-Quality Graphene *via* Microwave Reduction of Solution-Exfoliated Graphene Oxide. *Science* **2016**, *353*, 1413-1416.
(54) Dreyer, D. R.; Park, S.; Bielawski, C. W.; Ruoff, R. S. The Chemistry of Graphene Oxide. *Chem. Soc. Rev*. **2010**, *39*, 228-240.
(55) Larciprete, R.; Fabris, S.; Sun, T.; Lacovig, P.; Baraldi, A.; Lizzit, S. Dual Path Mechanism in the Thermal Reduction of Graphene Oxide. *J. Am. Chem. Soc*. **2011**, *133*, 17315-17321.
(56) Liu, L.; Tan, C. L.; Chai, J. W.; Wu, S. X.; Radko, A.; Zhang, H.; Mandler, D. Electrochemically "Writing" Graphene from Graphene Oxide. *Small* **2014**, *10*, 3555-3559.
(57) Chen, J.; Shepherd, R. L.; Razal, J. M.; Huang, X.; Zhang, W. M.; Zhao, J.; Harris, A. T.; Wang, S.; Minett, A. I.; Zhang, H. Scalable Solid-Template Reduction for Designed Reduced Graphene Oxide Architectures. *ACS Appl. Mater. Interfaces* **2013**, *5*, 7676-7681.
(58) Bagri, A.; Mattevi, C.; Acik, M.; Chabal, Y. J.; Chhowalla, M.; Shenoy, V. B. Structural Evolution during the Reduction of Chemically Derived Graphene Oxide. *Nat. Chem*. **2010**, *2*, 581-587.
(59) Becerril, H. A.; Mao, J.; Liu, Z.; Stoltenberg, R. M.; Bao, Z.; Chen, Y. Evaluation of Solution-Processed Reduced Graphene Oxide Films as Transparent Conductors. *ACS Nano* **2008**, *2*, 463-470.
(60) Wang, S.; Ang, P. K.; Wang, Z. Q.; Tang, A. L. L.; Thong, J. T. L.; Loh, K. P. High Mobility, Printable, and Solution-Processed Graphene Electronics. *Nano Lett*. **2010**, *10*, 92-98.